Geochemistry Geophysics Geosystems G3
AN ELECTRONIC JOURNAL OF THE EARTH SCIENCES
Published by AGU and the Geochemical Society

Article
Volume 10, Number 8
1 August 2009
Q08001, doi:10.1029/2009GC002378
ISSN: 1525-2027

Click Here for Full Article

Generation of plate-like behavior and mantle heterogeneity from a spherical, viscoplastic convection model

Bradford J. Foley
Department of Earth Sciences, University of Southern California, Los Angeles, California 90089, USA

Now at Department of Geology and Geophysics, Yale University, New Haven, Connecticut 06520, USA (bradford.foley@yale.edu)

Thorsten W. Becker
Department of Earth Sciences, University of Southern California, Los Angeles, California 90089, USA

[1] How plate tectonics arises from mantle convection is a question that has only very recently become feasible to address with spherical, viscoplastic computations. We present mainly internally heated convection results with temperature-dependent viscosity and explore parts of the Rayleigh number (Ra)–yield stress (σ_y) phase space, as well as the effects of depth-dependent σ_y, bottom heating, and a low-viscosity asthenosphere. Convective planform and toroidal-poloidal velocity field ratio (TPR) are affected by near-surface viscosity variations, and TPR values are close to observed values for our most plate-like models. At the relatively low convective vigor that is accessible at present, most models favor spherical harmonic degree one convection, though models with a weaker surface viscosity form degree two patterns and reproduce tomographically observed power spectra. An asthenospheric viscosity reduction improves plate-like nature, as expected. For our incompressible computations, pure bottom heating produces strong plumes that tend to destroy plates at the surface. This implies that significant internal heating may be required, both to reduce the role of active upwellings and to form a low-viscosity zone beneath the upper boundary layer.

Components: 8735 words, 12 figures, 1 table.

Keywords: plate tectonics; mantle dynamics; mantle convection; rheology; mantle structure.

Index Terms: 8120 Tectonophysics: Dynamics of lithosphere and mantle: general (1213); 8162 Tectonophysics: Rheology: mantle (8033); 8159 Tectonophysics: Rheology: crust and lithosphere (8031).

Received 8 January 2009; **Revised** 11 May 2009; **Accepted** 24 June 2009; **Published** 1 August 2009.

Foley, B. J., and T. W. Becker (2009), Generation of plate-like behavior and mantle heterogeneity from a spherical, viscoplastic convection model, *Geochem. Geophys. Geosyst.*, *10*, Q08001, doi:10.1029/2009GC002378.

1. Introduction

[2] Plate tectonics, the fundamental process that governs the solid Earth, is physically poorly understood. Plates form the upper boundary layer of thermal convection in the mantle and are themselves part of the mantle system, not objects passively moved by the mantle [*Tackley*, 2000c; *Bercovici et al.*, 2000; *Bercovici*, 2003]. However, plate tectonics is very different from the simplest (isoviscous, bottom heated) form of convection. For example, downwellings form antisymmetric,

sheet-like slabs, toroidal motion is prominent, deformation localizes at the boundaries of rigid plates, and the wavelength of coherent motion is very long.

[3] A key aspect of mantle convection is rock rheology. If viscosity is temperature-dependent, surface motion becomes coherent, but at high viscosity contrasts, $\geq 10^4$, the surface freezes up and becomes too strong to sink back into the mantle. This is termed stagnant lid convection, and is analogous to having one, motionless plate covering the entire globe [*Christensen*, 1984; *Ogawa et al.*, 1991; *Solomatov*, 1995]. The stagnant surface layer can be broken by adding plastic yielding to viscous, temperature-dependent models [e.g., *Moresi and Solomatov*, 1998]. In 3-D, Cartesian domains this rheology has been shown to break the stagnant lid and approximate plate tectonics [*Trompert and Hansen*, 1998; *Tackley*, 2000a, 2000b; *Stein et al.*, 2004]. Although these models are effective at focusing deformation into narrow weak zones surrounding rigid plates, they have several limitations. The range of yield stress values that produce plate-like behavior is relatively narrow, and values are of the order of 100 MPa [*Tackley*, 2000a, 2000b; *Stein et al.*, 2004], significantly lower than experimentally determined yield stresses for mantle rocks, which are of the order of 1000 MPa [e.g., *Kohlstedt et al.*, 1995]. The toroidal-poloidal velocity field ratio (TPR) was generally in the range of 0.25 to 0.35, with some models reaching 0.45 [*Tackley*, 2000a, 2000b; *Stein et al.*, 2004], lower than what is estimated for Earth in the last 120 Ma ($\sim$0.5 to 0.6 using plate motions from *Lithgow-Bertelloni et al.* [1993]). (We quote all TPR values without the net rotation component because the latter may be due mainly to continental keels [e.g., *Ricard et al.*, 1993; *Zhong*, 2001; *Becker*, 2006], and those are absent in our models.) Finally, these models tend to form the longest convective wavelength possible in their domain, while Earth forms a spherical harmonic degree two pattern (Figure 1) when inferred from seismic tomography [e.g., *Masters et al.*, 1982; *Su and Dziewonski*, 1991; *Becker and Boschi*, 2002].

[4] Most previous viscoplastic studies have been performed in Cartesian domains [*Tackley*, 2000a, 2000b; *Stein et al.*, 2004], though results for spherical models in a limited parameter space have recently been presented [*van Heck and Tackley*, 2008; *Walzer and Hendel*, 2008; *Yoshida*, 2008]. Aside from more realistically representing the Earth, spherical geometry should increase the amount of toroidal motion [*Bercovici*, 1993]. Previous models in both Cartesian and spherical geometry have examined narrow *Ra* ranges, and the affect of differing heating modes has not been fully explored. We present a somewhat extended exploration of the Ra-σ_y phase space, as well as comparisons between models with constant and depth-dependent σ_y, different heating modes, and an asthenospheric viscosity reduction, as this has been found to promote plate-like motion [*Tackley*, 2000b], and a tendency for longer-wavelength flow in 2-D [*Chen and King*, 1998; *Han and Gurnis*, 1999], and in 3-D [*Richards et al.*, 2001; *Busse et al.*, 2006; *Hoeink and Lenardic*, 2008].

2. Methods

2.1. Model Setup

[5] All simulations were computed using the spherical shell convection code CitcomS [*Moresi and Solomatov*, 1995; *Zhong et al.*, 2000; *Tan et al.*, 2006]. CitcomS is a finite element code that solves the governing equations for conservation of mass, momentum, and energy in a fluid under the Boussinesq approximation:

$$u_{i,i} = 0 \tag{1}$$

$$-P_{,i} + \left(\eta u_{i,j} + \eta u_{j,i}\right)_{,j} + RaT\delta_{ir} = 0 \tag{2}$$

$$T_{,t} + u_i T_{,i} = T_{,ii} + H. \tag{3}$$

Here u is velocity, P is dynamic pressure, η is viscosity, Ra is the Rayleigh number, T is temperature, and H is heat production rate in the nondimensionalized form of *Zhong et al.* [2000]. The term $X_{,y}$ means the derivative of X with respect to y, with i and j representing spatial indices, r representing the radial direction, and t representing time. This nondimensionalization uses the radius of Earth, R, as the length scale. However, for easier comparison with other studies, we will state actual values for the Rayleigh number in the more convectional manner, using the thickness of the mantle, D, as the length scale. This Rayleigh number is defined as:

$$Ra_D = \rho_o g \alpha \Delta T D^3/(\kappa\eta_o) = (D/R)^3 Ra, \tag{4}$$

where κ is thermal diffusivity, η_0 is reference viscosity, ρ_0 is reference density, ΔT is temperature difference from the CMB to the surface, g is acceleration due to gravity, and α the coefficient of thermal expansion.

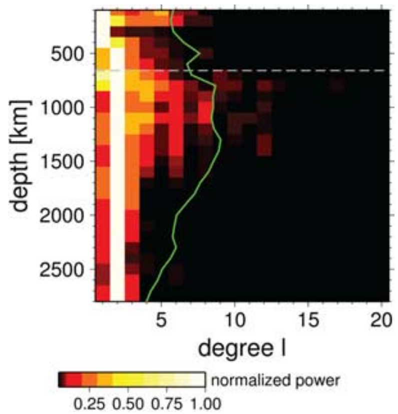

Figure 1. Normalized power spectrum plot for shear wave velocity anomalies in tomography model S20RTSb by *Ritsema et al.* [2004]. Spectral power in each depth range is normalized by maximum power per degree to emphasize the relative spectral character. Green line indicates first moment of power, and dashed gray line indicates 660 km for reference (see *Becker and Boschi* [2002] for details).

[6] Our Ra_D, which varies from 9×10^4 to 9×10^5, is approximately a factor of 100 lower than typical estimates for Earth but is comparable to other Cartesian and spherical models [*Tackley*, 2000a, 2000b; *van Heck and Tackley*, 2008]. Higher Rayleigh numbers were not accessible in a systematic fashion because of computational constraints. We scaled stress using a reference viscosity of 10^{23} Pas for an Ra_D of 9×10^4. To increase Rayleigh number the reference viscosity, being the least well-constrained parameter, is lowered, affecting the stress scaling. For example, an Ra_D of 9×10^5 uses a reference viscosity of 10^{22} Pas.

[7] For most models, internal heating with $H = 60$ was used, which scales to $\sim$7 TW. Also, a zero heat flux bottom boundary condition and mechanically free slip top and bottom boundaries were used. The Rayleigh number as defined in (4) assumes an imposed temperature difference across the mantle, while our internal heating setup uses a uniform heat generation rate. It is common to define a Rayleigh number based on internal heating rate, Ra^H, based on the thermal gradient at the top boundary layer [e.g., *Davies*, 1999], which leads to the equivalence, $Ra_D^H = Ra_D H_D$ for Cartesian geometry [*Tackley*, 2000a], and $Ra^H = Ra \times H \times (1 - r^3)/3$ for spherical geometry where r is the radius of the outer core divided by the radius of the Earth. For heating mode tests, the thermal bottom boundary condition was switched to isothermal, and various levels of internal heating were used. Using the scaling between Ra_H and Ra, we increased our Ra for purely bottom heated models by approximately an order of magnitude so models had a comparable convective vigor.

[8] Our temperature-dependent viscosity formulation follows *Tackley* [2000a, 2000b]:

$$\eta = \eta_o \exp(\eta_e/(T + \eta_T) - \eta_e/(1 + \eta_T)). \tag{5}$$

We use $\eta_0 = 1$, $\eta_e = 18.43$ and $\eta_T = 1$, which gives a four order of magnitude viscosity contrast from nondimensional temperatures of 0 to 1. Using slightly stronger temperature dependence as in the works by *Tackley* [2000a, 2000b] causes numerical problems. To ensure that viscosity contrasts do not become to large for the code to converge on a solution, viscosities for the whole system are clipped at $\log(\eta) = -1$ and 4, as the lower value can be reached at temperatures greater than 1. The resulting average viscosity of the mantle is usually between 1×10^{21} and 1×10^{22}. The last piece of the rheology used is plasticity, governed by a "Byerlee" type yield stress relation:

$$\sigma_y = \min(a + b(1 - r), c). \tag{6}$$

Here, a is cohesion and b a depth-dependent factor, giving a failure envelope for "brittle" behavior, similar to Byerlee's "Law" [e.g., *Schott and Schmelling*, 1998; *Tackley*, 2000a]. It is clear that a fluid treatment such as ours cannot fully capture the micromechanics of faulting and σ_y is merely a proxy for a range of weakening processes. For "ductile" behavior, c is used to prescribe a constant yield stress throughout the mantle. Experiments combining ductile and brittle behavior are termed depth-dependent yield stress experiments, while those with just ductile behavior are termed constant yield stress experiments. For depth-dependent σ_y tests a constant cohesion term is used, and the frictional gradient term is set to 20 times the constant, "ductile" term, giving "brittle" behavior for the upper 1/20th of the mantle, or approximately 150 km. Viscosity is then recalculated as follows:

$$\eta_y = \sigma_y / 2\dot{e}_{II} \tag{7}$$

$$\eta_{eff} = \eta \cdot \eta_y / \left(\eta + \eta_y\right), \tag{8}$$

where η is the previously calculated viscosity, and $\dot{e}_{II}$ is the second invariant of the strain rate tensor:

$$\dot{e}_{II} = \left[1/2\Sigma_{ij}\dot{e}_{ij}\,\dot{e}_{ij}\right]^{1/2}. \tag{9}$$

A summary of the models presented in this paper, including their key parameters and diagnostics, is presented in Table 1.

[9] We used a resolution of 32 × 32 × 32 × 12 elements for low Ra_D models (9×10^4), and 64 × 64 × 64 × 12 for higher Ra_D models (2.8×10^5 and higher). We also used vertical refinement in the boundary layers, where 20% of the nodes are placed in the top 10% of the domain, and 15% of the nodes are placed in the bottom 10% of the domain. Comparisons of key diagnostics, such as surface heat flow, with an increased resolution test with 64 × 64 × 64 × 12 for low Ra_D models and 128 × 128 × 128 × 12 for high Ra_D models showed the same general time dependence and convective character (see Appendix A). While details of the computations differ, we therefore expect that the results shown for the more computationally tractable lower resolutions are stable in terms of their gross characteristics.

2.2. Plate Diagnostics and Comparison With Heterogeneity Spectra From Mantle Tomography

[10] For analysis of toroidal motion and convective wavelength, a spherical harmonic expansion of the surface velocities up to degree and order 63 was used. The velocity field can then be separated into toroidal and poloidal components, and the TPR is computed as the ratio of respective RMS powers, with net rotation removed. The TPR analysis can also be compared to Earth using *Lithgow-Bertelloni et al.*'s [1993] compilation of plate reconstructions for the last 120 Ma, leading to the aforementioned range of 0.5 to 0.6. Spatial power spectra of temperature from spherical harmonics depict the wavelengths of convection and can be compared to velocity anomaly spectra estimated from seismic tomography [e.g., *Tackley*, 1996; *Bunge et al.*, 1996], and all definitions here are as in the work by *Becker and Boschi* [2002]. The mapping between seismic tomography and temperature spectra is, of course, nontrivial [e.g., *Megnin et al.*, 1997; *Tackley*, 2006; *Ritsema et al.*, 2007]. However, for our qualitative comparisons we will neglect issues such as imperfect resolution.

[11] To allow for comparisons to *Tackley* [2000a, 2000b], we also included the diagnostics "plateness" and "mobility." Mobility measures the amount of surface motion compared to the velocity throughout the rest of the mantle. Convection should have the highest velocities in the boundary layers and horizontal motions on the surface should be higher than motion in the rest of the mantle, unless the surface is stagnant. We measure this in following with *Tackley* [2000a]:

$$M = v_{rms\_surface} / v_{rms\_whole}. \tag{10}$$

Plateness attempts to measure the style of plate formation by determining how small an area the largest strain rates are confined to. We measured the area that contains 80% of the strain at the surface ($f80$) but find that $f80$ is problematic because very small strains take place over a large area in our models and end up contributing significantly to the total strain. To account for this, strain rates that were 3% or less of the maximum strain rate were not counted in the strain summation. We then normalize the diagnostic by measuring the average $f80$ for an isoviscous model, which was found to be 30% of the surface. Plateness is then determined by:

$$P = 1 - f80/0.3. \tag{11}$$

3. Results

3.1. Cartesian Results

[12] Previous work has been done in 2-D Cartesian domains that produces some features of plate tectonics, such as coherent surface motion [e.g., *King and Hager*, 1990; *Weinstein and Olson*, 1992], and 3-D models often show similar features [*Stein et al.*, 2004; *Tackley*, 2000a, 2000b]. However, the truest test of plate generation is in 3-D spherical geometry, since this ensures a lack of imposed symmetries, and is most representative of the Earth. Before moving to spherical geometry, the use of Citcom for viscoplastic convection was tested by reproducing *Tackley*'s [2000a, 2000b] Cartesian experiments using the Cartesian CitcomCU [*Moresi and Solomatov*, 1995; *Zhong et al.*, 1998]. We had to use a slightly different model set up in that reflective boundary conditions were applied instead of the periodic boundary conditions used by *Tackley* [2000a, 2000b]. Our models, at an $Ra_D = 10^5$, showed a narrow range of σ_y for plate-like behavior when a constant yield stress was used (∼20–35 MPa), and a wider range of σ_y when depth-dependent yield stress was used (∼20–85 MPa). Using depth-dependent yield stress changed the plate-like σ_y range, while for *Tackley* [2000a] it did not; his plate-like range was ∼50–120 MPa. The width of σ_y producing plate-like behavior for depth-dependent yield stress was, however, similar to *Tackley*'s [2000a]. These differ-

Table 1. A Summary of Constant and Depth-Dependent Yield Stress Models[a]

Constant Yield Stress Model	Ra_D	σ_y (MPa)	Internal Heating	Average Velocity	Average P	Average M	Average TPR	Regime	Dominant Degree
Run 1	9×10^4	25	100%	369.3 ± 244.8	0.92 ± 0.03	1.48 ± 0.12	0.29 ± 0.08	Mobile	2
Run 2	9×10^4	125	100%	237.4 ± 96.2	0.84 ± 0.06	1.27 ± 0.04	0.36 ± 0.07	Plates	1
Run 3	9×10^4	212.5	100%	296.5 ± 244.7	0.79 ± 0.07	1.16 ± 0.16	0.30 ± 0.11	Episodic	1
Run 4	9×10^4	625	100%	4.1 ± 11.5	0.98 ± 0.00	0.08 ± 0.03	0.19 ± 0.08	Stagnant	N/A
Run 5	9×10^4	162.5	100%	210.4 ± 100.5	0.79 ± 0.11	1.24 ± 0.09	0.36 ± 0.08	Plates	1
Run 6	5.6×10^5	83.3	100%	399.4 ± 146.8	0.89 ± 0.03	1.34 ± 0.07	0.41 ± 0.08	Plates	2
Run 7	9×10^5	75	100%	428.5 ± 178.5	0.90 ± 0.05	1.34 ± 0.09	0.44 ± 0.05	Plates	1 and 2
Run 8	9×10^5	125	100%	443.0 ± 206.9	0.96 ± 0.02	1.22 ± 0.17	0.42 ± 0.10	Plates	1
Depth-Dependent Yield Stress Model	Ra_D	σ_y (MPa)	Internal Heating	Average Velocity	Average P	Average M	Average TPR	Regime	Dominant Degree
Run 9	9×10^4	120	100%	219.2 ± 53.1	0.75 ± 0.03	1.41 ± 0.03	0.32 ± 0.06	Plates	2
Run 10	9×10^4	240	100%	198.7 ± 66.3	0.73 ± 0.03	1.34 ± 0.03	0.33 ± 0.08	Plates	1
Run 11	5.6×10^5	116.7	100%	271.1 ± 23.1	0.80 ± 0.03	1.53 ± 0.04	0.35 ± 0.04	Plates	2
Run 12	9×10^5	95	100%	297.8 ± 39.8	0.78 ± 0.03	1.62 ± 0.06	0.31 ± 0.04	Plates	2
Heating Mode Test Model	Ra_D	σ_y (Nondimensional)	Internal Heating	Average Velocity	Average P	Average M	Average TPR	Regime	Dominant Degree
Run 13	5.6×10^6	1×10^6	0%	480.0 ± 130.5	0.68 ± 0.18	1.46 ± 0.12	0.15 ± 0.05	Mobile	2
Run 14	1.87×10^6	1×10^6	50%	697.7 ± 492.5	0.92 ± 0.03	0.92 ± 0.37	0.32 ± 0.03	Plates	1

[a] The models shown represent a subset of approximately 50 total computations. Runs 1–4 are shown in Figure 2, runs 5–8 are shown in Figure 7, runs 9–12 are shown in Figure 9, and runs 13–14 are shown in Figure 10.

ences can likely be explained by the use of different boundary conditions, and would not affect spherical models.

3.2. Spherical Results

3.2.1. Constant σ_y

[13] As *Tackley* [2000a, 2000b] and *Stein et al.* [2004] found for Cartesian, and *van Heck and Tackley* [2008] found for spherical geometry, there are four basic convective regimes. They are, with increasing yield stress: the mobile regime, the plate-like regime, the episodic regime, and the stagnant lid regime (Figure 2). We distinguish between these regimes by examining convective planform (temperature, viscosity, and velocity fields) in statistical steady state (generally after ~50,000 time steps), and the plate diagnostics as defined above.

[14] The mobile regime is found for low yield stress values (<100 MPa), and is characterized by a weak surface (Figure 3) due to extensive yielding resulting in tubular downwellings and incoherent surface motion. In addition, we find that TPRs are low (~0.3) because of the lack of large surface lateral viscosity variations, and that convective wavelength is short, since the surface is nearly everywhere weakened by yielding. The plate-like regime is found for higher σ_y (75–210 MPa at low Ra_D). This regime is characterized by linear, sheet-like downwellings with relatively narrow weak zones accommodating the majority of surface deformation, as well as smooth heat flux trends (Figure 4). We also find that TPRs peak during the plate-like case, at ~0.35 at low Ra_D, because of large lateral viscosity variations, and that the wavelength of the convection pattern is typically dominated by degree one and degree two patterns (Figures 2 and 7).

[15] With higher yield stress (210–250 MPa at low Ra_D), models become episodic; they switch between plate-like and stagnant lid behavior periodically through time. This regime is therefore characterized by periods of high and low heat flux. TPRs show this same variability (Figure 5), and convective wavelength is dominated by a degree one pattern during periods of mobility. Last, at high yield stress values (≥250 MPa), models enter the stagnant lid regime where the surface is immobile and never breaks to subduct back into the mantle. Convection takes place by short-wavelength, drip-like downwellings that form from small instabilities off the bottom of the stagnant upper boundary layer. TPRs are low and spectra show the most power in high degrees (10–15) occurring at upper mantle depths, corresponding to the short-wavelength pattern of the drip-like planform. These regimes are roughly the same as those seen by *van Heck and Tackley* [2008], who used an entirely different numerical method, though they differentiate different convective planforms within the plate-like regime.

[16] Using the above definitions, runs were classified as mobile, plate-like, episodic, or stagnant lid throughout the Ra_D-σ_y phase space (Figure 6). The range of σ_y that produces plate like behavior at $Ra_D = 9 \times 10^4$ is 75 to 210 MPa. *Tackley*'s [2000a, 2000b] Cartesian experiments, at this Ra_D, found a range of 50–125 MPa for plate-like models. We find a slightly wider range (135 MPa wide instead of 75 MPa wide), and a range shifted toward higher values. This phase space is very similar to that found by *van Heck and Tackley* [2008] for spherical geometry. We also find that at $Ra_D = 9 \times 10^5$, scaled values of 75 to 125 MPa produce plate-like behavior, so these regimes appear to be independent of *Ra*, when the viscosity scaling is applied.

[17] Substantiating the findings by *van Heck and Tackley* [2008], the planform of convection for viscoplastic models with a constant σ_y shows many features akin to plate tectonics on Earth (Figures 2 and 7). However, strike-slip style boundaries, when they form, are always diffuse. This may be due to lack of resolution or an incomplete rheology, perhaps because of the lack of memory of weakening [e.g., *Zhong et al.*, 1998]. Downwellings are sheet-like and usually symmetrical, though some form transient asymmetry because of trench roll-back (Figures 7c, 7d, 7g, 7h, 7k, and 7l). Triple junctions form frequently at ridge-ridge-ridge and trench-trench-trench locations, which are stable and conditionally stable, respectively [*McKenzie and Morgan*, 1969]. There are often offsets in ridges, though they are usually quite large, and not as extensive as the ridge and transform fault make up of Earth's divergent boundaries (Figures 7b, 7f, and 7j).

[18] The convective planform shows dependence on both σ_y and Rayleigh number. With increasing *Ra*, downwellings become more numerous and smaller, and more plates form (Figures 7b, 7c, 7f, 7g, 7j, and 7k), but as σ_y is increased, models tend to form just one major downwelling (Figures 7d, 7h, and 7l). However, these models have a tendency to leave portions of the sphere essentially immobile, as the smaller plate size is not matched by a

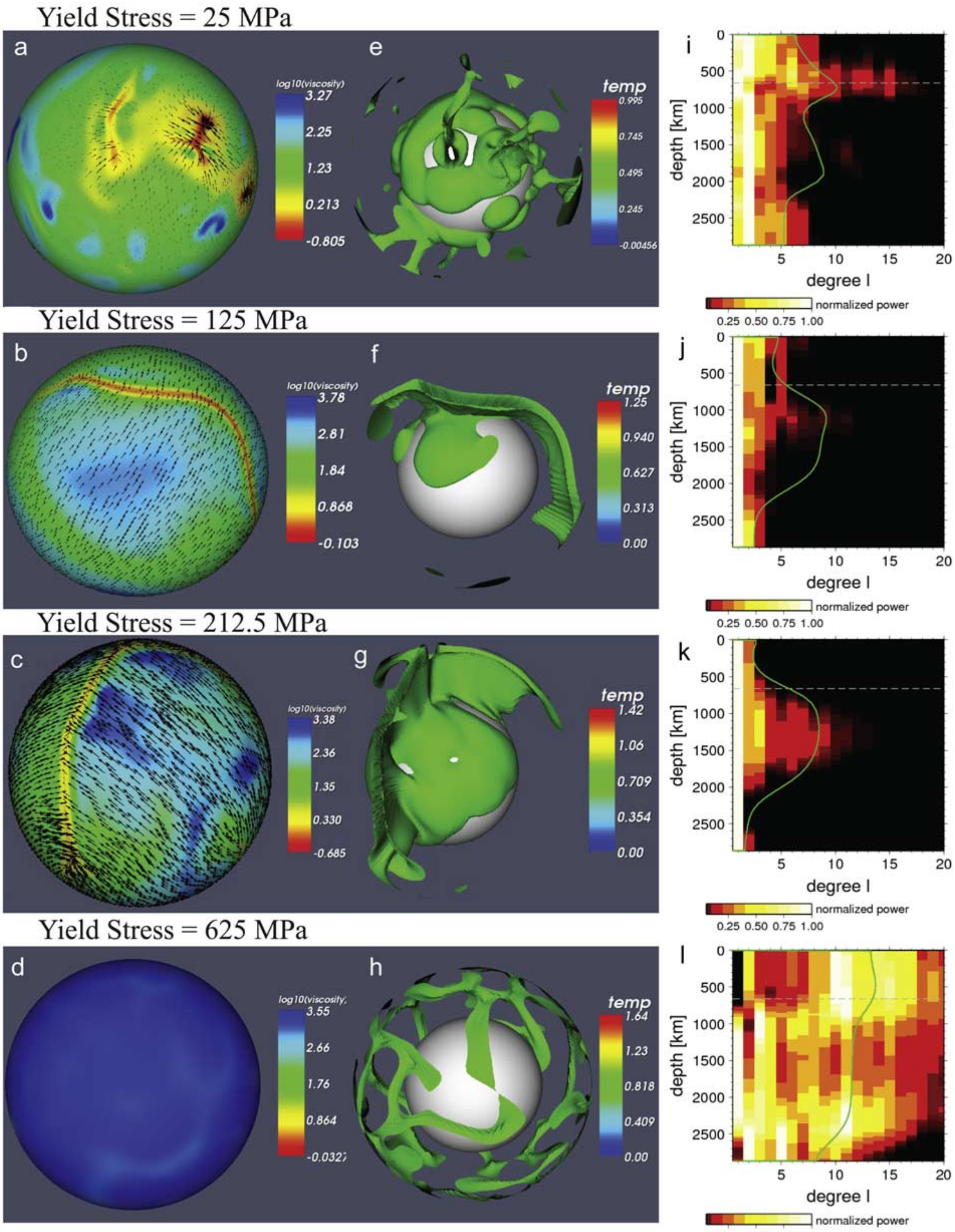

Figure 2. Low Ra_D, constant σ_y models. (a–d) Viscosity fields with velocity vectors, (e–h) cold (T $\sim$ 0.5) temperature isosurfaces, and (i–l) temperature power spectra for the four regimes of convection at $Ra_D = 9 \times 10^4$, with specified σ_y. Figures 2a, 2e, and 2i show mobile convection; Figures 2b, 2f, and 2j show plate-like convection; Figures 2c, 2g, and 2k show episodic convection; and Figures 2d, 2h, and 2l show stagnant lid convection.

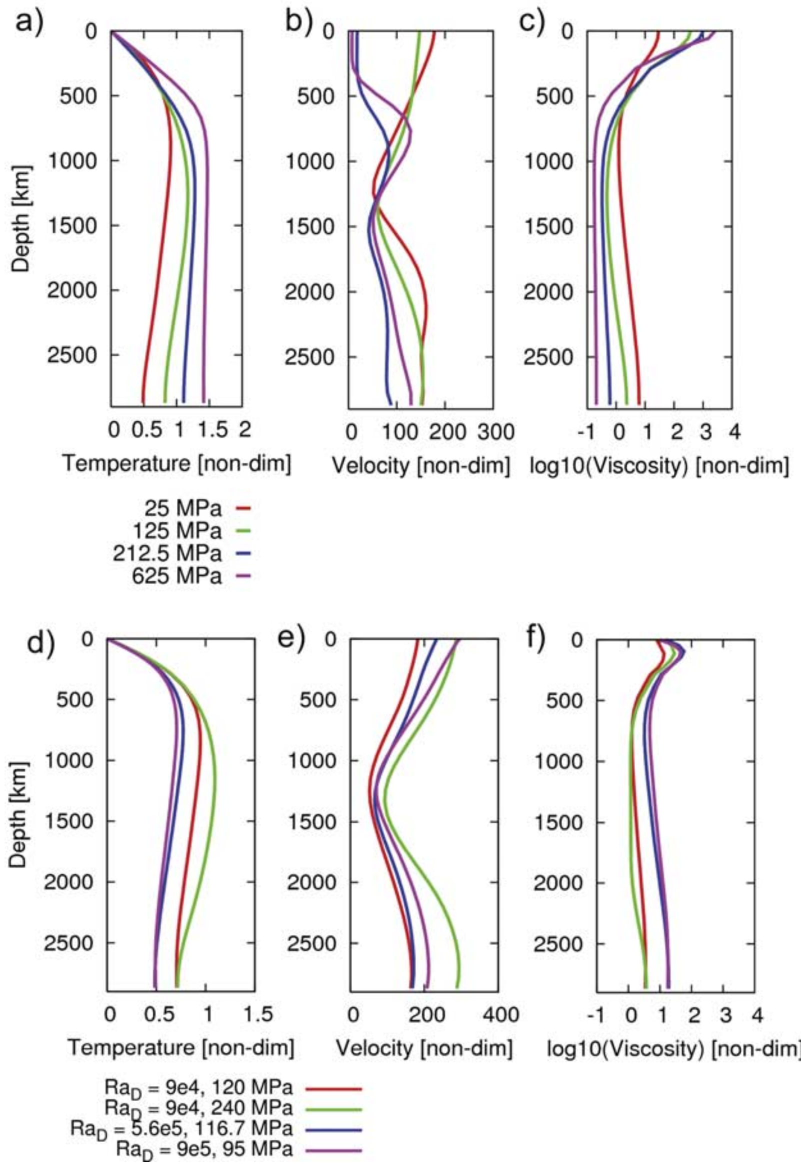

Figure 3. Horizontal averages of (a) temperature, (b) volume-averaged RMS velocity, and (c) viscosity with depth corresponding to the models shown in Figure 2. With this velocity measure, a nondimensional value of 200 scales to ~0.1 cm/a. Note how yielding causes different viscosity structures, especially at the surface, for the four different regimes. (d–f) Plots for the depth-dependent σ_y case (Figure 9).

comparable increase in downwellings. The decrease in lateral size of downwellings also causes plate boundaries to not link up, i.e., not form well-defined plates.

[19] *Tackley* [2000a, 2000b] found that viscoplastic models with a strongly temperature-dependent viscosity and low Rayleigh number in Cartesian domains tended to form a convection pattern with the largest possible wavelength. We find that similarly, the longest-wavelength pattern is favored for most plate-like models. Such behavior was also recently pointed out by *Zhong et al.* [2007] for temperature-dependent viscosity cases that do not result in a stagnant lid, and *Hoeink and Lenardic* [2008] when a low-viscosity asthenosphere is used. However, we also find that increasing *Ra* causes a decrease in convective wavelength, but dominant degrees are still $\leq$4. The opposite effect is found for σ_y, where an increase causes an increase in the wavelength of convection (Figure 7). Therefore a narrow range of models, with low σ_y and medium to high Rayleigh number, form degree 2 patterns. Outside of this region, degree one convection is the presiding pattern. Degree 2 convection was also found by *Yoshida* [2008] for low yield stress

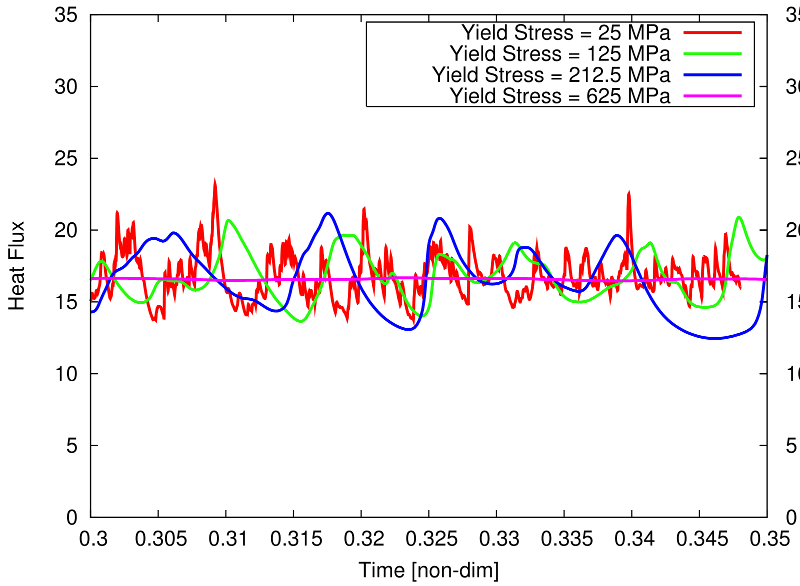

Figure 4. Nondimensional surface heat flux for the models shown in Figure 2. The time span of 0.05 shown scales to ∼60 Ga, with a sampling of 100 Ma. However, this large time scale is due to our *Ra* being low compared to Earth. A nondimensional heat flux of 20 scales to ∼15 mW/m^2.

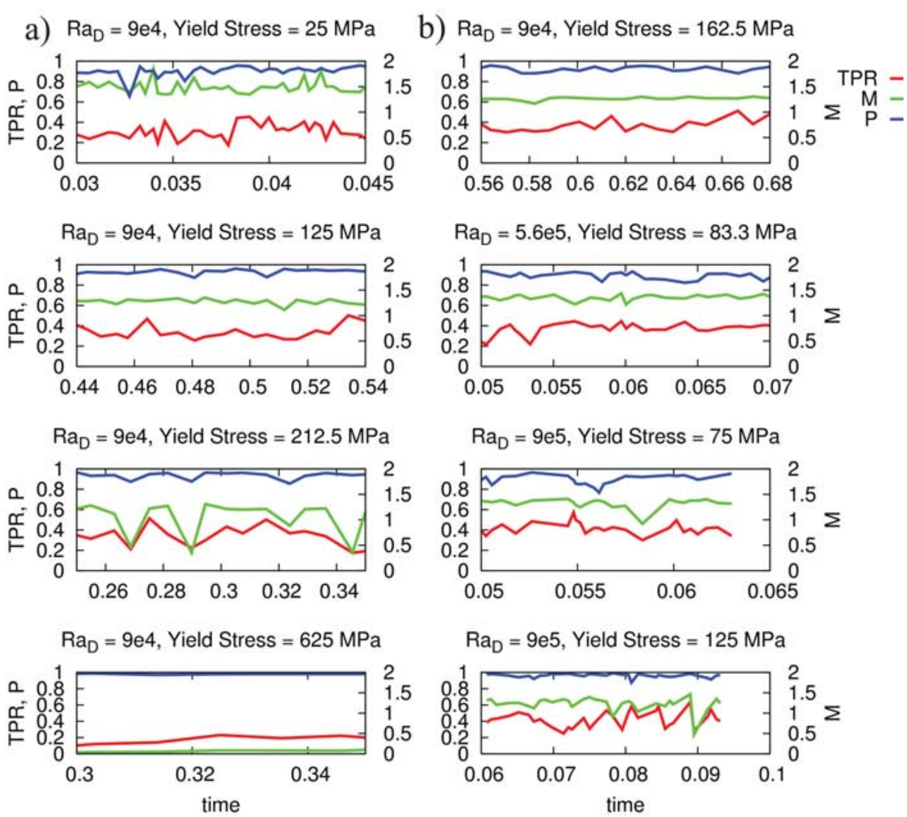

Figure 5. (a) Plate diagnostics through time for the four regimes shown in Figure 2, i.e., the low Ra_D, constant σ_y case. As before, 0.05 nondimensional time scales to ∼60 Ga. Time sampling is dependent on model parameters but is generally of the order of 5 Ga, clearly hiding shorter-term fluctuations. (b) Same plots for the high Ra_D, constant yield stress case (Figure 7).

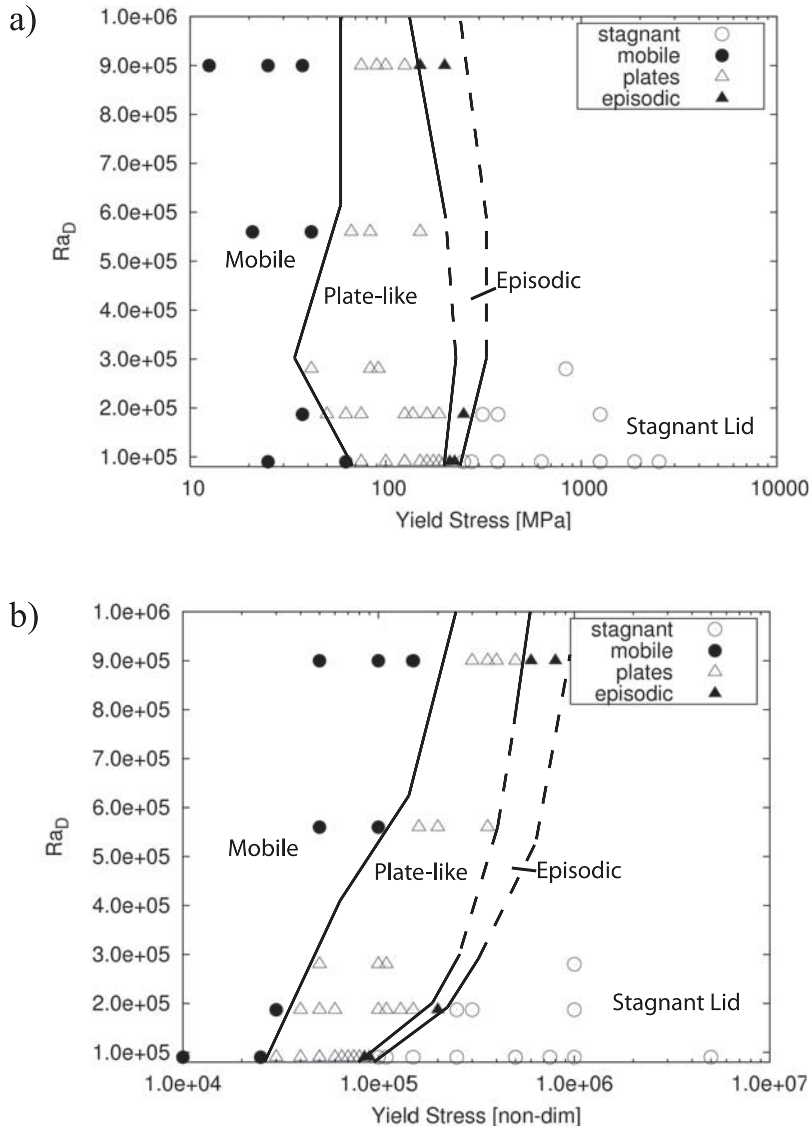

Figure 6. Phase space plot of the four regimes of convection in Ra_D-σ_y phase space with (a) scaled yield stress using variable viscosity (see section 2.1) and (b) nondimensional yield stress.

parameters, and an apparent degree 2 planform was observed by *van Heck and Tackley* [2008], also for low yield stress values.

[20] At a constant Ra_D, mobility shows a steady decrease from mobile regime models to stagnant lid regime models (Figure 8). The standard deviation of mobility is high for mobile models, then low for plate-like models, and increasing for episodic models. This helps outline the plate-like regime, which by definition has less variability of surface motion, and therefore a lower standard deviation, than both the mobile and episodic regimes. Surface velocities in the plate like range are generally between nondimensional values of 200–600 (Table 1), which scales to ~0.1–0.3 cm/a.

[21] Plateness has similar trends in σ_y space, and no discernible Rayleigh number dependence (Figure 8). Plate-like models show a plateness of between 0.85 and 0.95, with low variability through time. Episodic cases have a lower P, ranging from 0.7 to 0.85, and higher variability. Counter intuitively, the mobile regime shows very high P. This is caused by the way deformation takes place in a few small, tubular downwellings, concentrating most of the strain in the system in the small area these downwellings take up. So even though plates do not form, the deformation is localized to a small area on the surface.

[22] Toroidal-poloidal ratios (TPRs) range between 0.2 and 0.6 through time for plate-like models

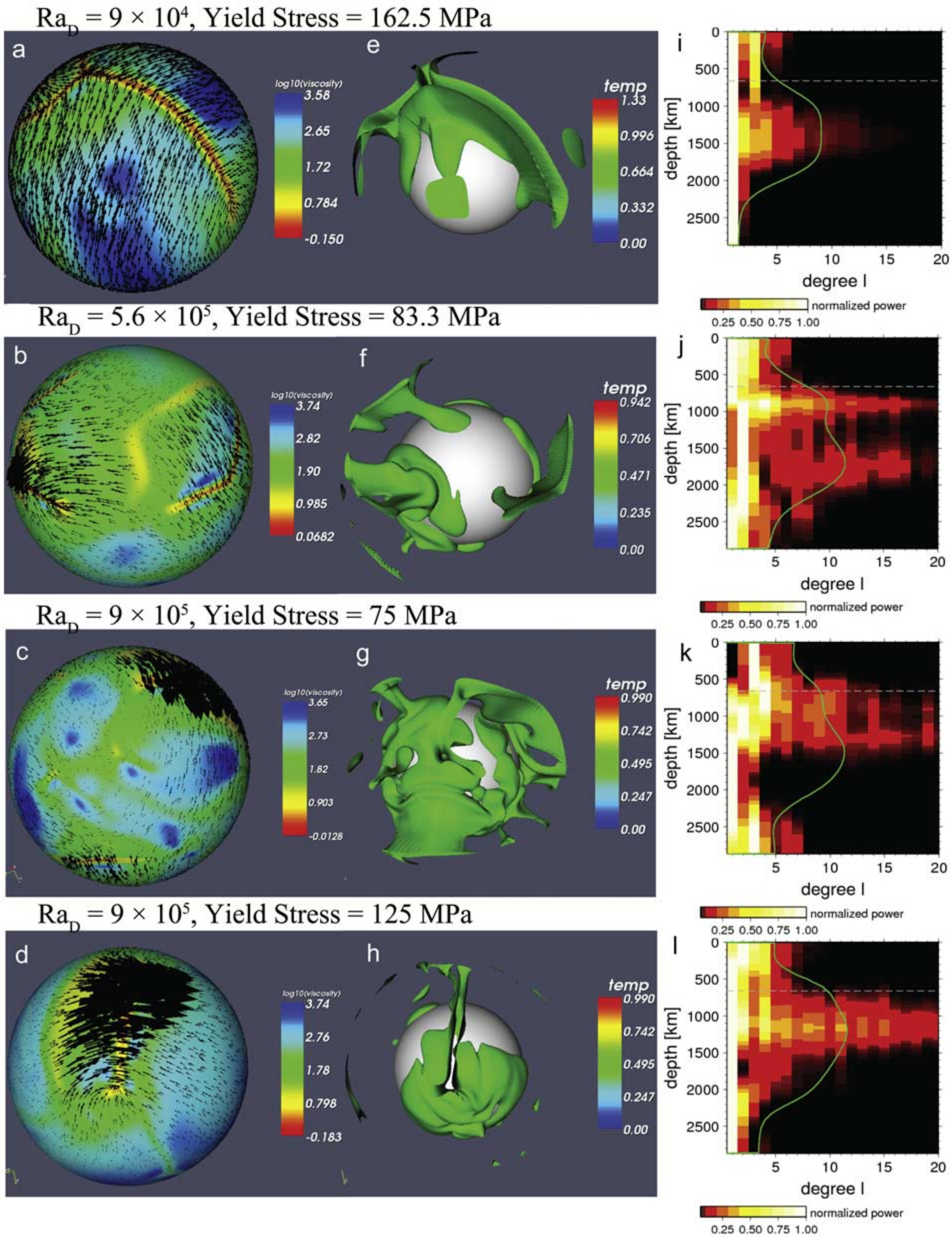

Figure 7. Convective planform for the plate-like, high Ra_D, constant σ_y case, with images shown in the same manner as Figure 2.

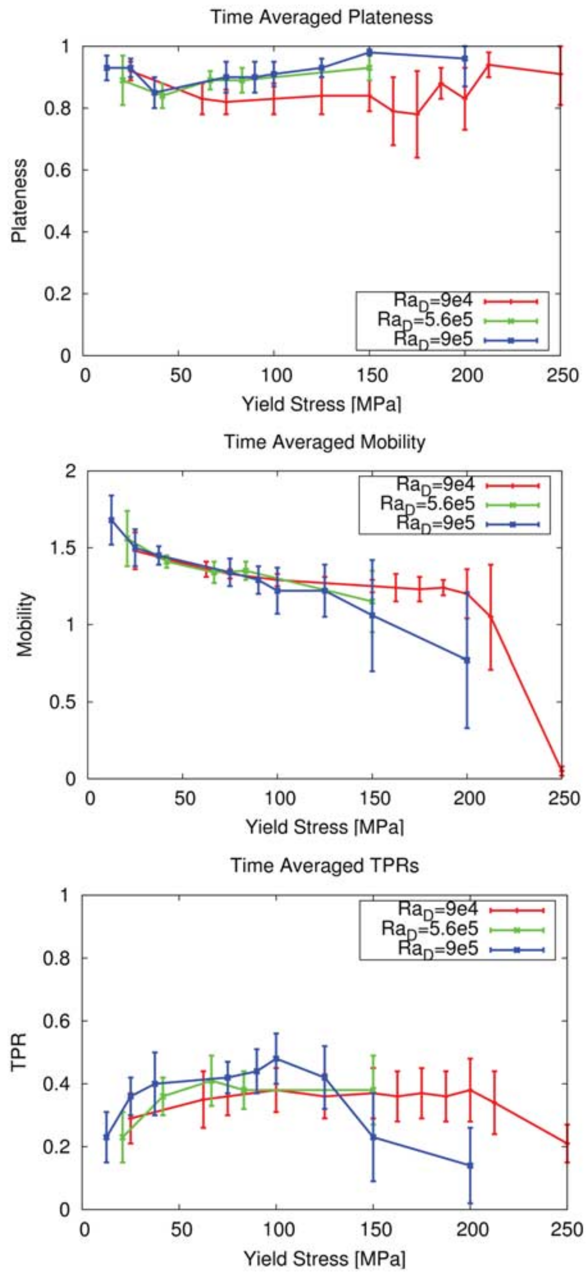

Figure 8. Time-averaged (top) plateness, (middle) mobility, and (bottom) TPR for models at Ra_D as specified.

(Figure 5), with some oscillation about the mean, though the time dependence is undersampled because we could not record output as frequently as necessary because of storage constraints, so any high-frequency signals are lost (Figures 4 and 5). *Van Heck and Tackley* [2008] see similar results, with TPRs for plate-like models ranging from 0.25 to 0.4 for Ra_D = 10^5. TPRs were also time averaged, and plotted in TPR-σ_y phase space at various Ra_D (Figure 8), providing an outline of the plate-like regime in Ra_D-σ_y parameter space. TPR is an effective measure of plate tectonic style convection because toroidal motion is strongly linked to lateral viscosity variations in the surface layer, which are largest for plate-like models. Furthermore, we find an increase in TPR with increased *Ra*, from time averages of 0.37 for $Ra_D = 9 \times 10^4$ to 0.44 for $Ra_D = 9 \times 10^5$. Though this effect is small, it may become more pronounced with increased *Ra*. Increasing Rayleigh number should cause an increase in TPR, as a more vigorous convection should increase lateral viscosity variations.

3.2.2. Depth-Dependent σ_y

[23] Since pressure has a strong effect on yield strength, a depth-dependent σ_y was tested. This rheology attempts to model Byerlee's "Law" with a linearly increasing σ_y in the upper mantle and a constant σ_y in the rest of the mantle. In Cartesian geometry this rheology produces a weaker surface with sharper zones of deformation [*Tackley*, 2000a]. Results following *Tackley* [2000a] for depth-dependent σ_y produce shorter-wavelength structures, sharper zones of deformation (Figure 9), but lower TPRs because the surface has a lower viscosity, and hence smaller lateral viscosity variations. The plate-like σ_y range also changes, shifting to higher values because of the depth dependence of the σ_y through the lithosphere which effectively weakens the surface and facilitates formation of downwellings. At low $Ra_D = 9 \times 10^4$, models with 500 and 625 MPa average σ_y produce plate-like behavior, instead of the stagnant lid behavior these parameters form with a constant σ_y.

[24] Using a depth-dependent σ_y weakens the surface by as much as one order of magnitude as compared to constant σ_y cases with similar parameters (Figures 3d–3f). This weaker surface allows downwellings to form and shorter-wavelength convection patterns result (Figure 9). In general, plate boundaries are narrower and weaker. There are fewer areas of internal deformation as compared to constant yield stress experiments, and plates form more coherently. Spreading ridges often show offsets and triple junctions, and oblique spreading, but no distinct transforms form. Convergent boundaries also tend to form complex geometries, such as offsets and triple junctions. Downwellings usually cluster on one side of the globe, leaving the other side broken into spreading ridges. However, the strict degree one pattern of one divergent boundary and one convergent boundary does not form.

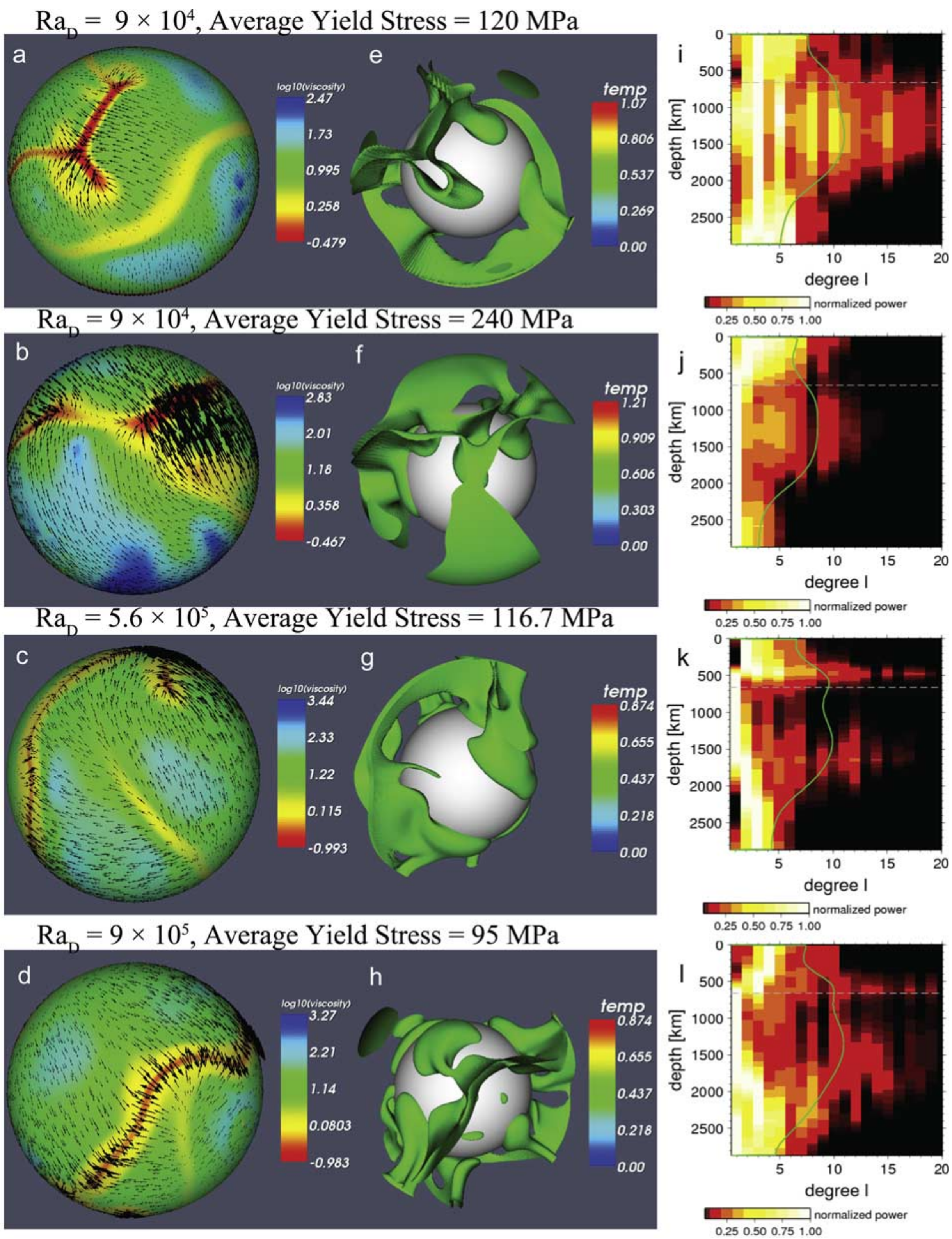

Figure 9. Convective planform (as in Figure 2) for the depth-dependent σ_y case. Compare Figures 9a, 9e, and 9i to Figures 2b, 2f, and 2j.

[25] Power spectra show a roughly one degree shift compared to the constant σ_y model (Figure 9). Models with moderate to low σ_y at low Rayleigh number now show strong degree two signals, as well as high power up to degree five. With increasing *Ra*, these models are dominated by degree two and degree three power. At high σ_y, degree one is still dominant, but there is power in degrees two to five as well, significantly higher than in constant σ_y cases. This shift to lower wavelength is caused by the ease with which downwellings form. The lower yield stress at the surface allows for lower stress levels to break the stagnant lid and initiate subduction.

[26] TPRs are lower than for constant σ_y models because lateral viscosity variations are smaller. Depth-dependent σ_y models have a TPR approximately 0.05 lower than the equivalent constant σ_y experiment, and variability through time is generally the same. Plateness is also lower than for constant σ_y runs (0.75 as compared to 0.85), despite the finding that the surface viscosity field appears more plate-like. This is probably due to the increased number of downwellings, leading to a higher surface area with high strain rates, and therefore increasing $f80$. Variability through time is the same or lower for depth-dependent σ_y. Mobility is significantly higher, $\sim$0.2, on average when compared to corresponding constant σ_y cases. This is also caused by the increase in downwellings, which, through slab pull, lead to higher surface mobility.

[27] Another way to model the effects of pressure on yield strength is to set σ_y to only act on the lithosphere and upper mantle, since increasing pressure should increase the strength of rocks and make yielding unlikely in the lower mantle. Our constant σ_y models and depth-dependent σ_y models discussed above show some yielding when downwellings impinge on the CMB. Using a rheology with σ_y confined to the upper mantle, models show a less time-dependent convective planform, higher TPR values by as much as $\sim$0.1, more plate-like surface motions, and similar power spectra when compared to the corresponding model with a constant σ_y throughout the mantle. These effects are due to a stabilization of the planform, since downwellings no longer yield in the lower mantle.

3.2.3. Heating Mode Tests

[28] The Earth has both internal heating, from radioactive decay, and bottom heating, from heat flux through the CMB [e.g., *Lay et al.*, 2008]. Bottom heated models, with reduced rates of internal heating, H, were run to explore the effect of heating modes on plate generation.

[29] For pure bottoming heating at an $Ra_D = 5.6 \times 10^6$, which lies between the range of Ra_D^H used for the purely internally heated models (7×10^5 to 7×10^6), we do not observe plate-like surface features, because plumes tend to destroy plates (Figure 10a). The surface above a plume yields and weakens sharply, and velocity within this zone is radial outward from the center of the plume head. Instead of forming linear spreading ridges, the surface is being pushed apart from points. Outside of the spreading region, the surface strengthens and moves in a more plate-like manner toward linear, sheet-like subduction zones. These downwellings form a series of interconnected rings around the plumes similar to the low *Ra* steady state patterns of spherical convection [e.g., *Bercovici et al.*, 1989]. These models have a very low plateness ($\sim$0.65), because of the large areas of the surface undergoing high strain from plume interaction with the lithosphere, and a high mobility ($\sim$1.45), because the plumes are contributing a force to surface motion that is nonexistent in internally heated models. TPRs are also very low, $\sim$0.15; that is, the system is almost purely poloidal because large internal deformation within the plates occurs.

[30] The viscosity and temperature structures for pure bottom heating and pure internal heating are very different, as expected. With internal heating, the mantle has a high average temperature ($\sim$1) and therefore low average viscosity. With bottom heating, the average mantle temperature (outside of the boundary layers) is $\sim$0.5. This causes a lower average viscosity contrast between the surface and underlying mantle. Using a portion of internal heating that creates a warmer average mantle, especially just below the upper boundary layer (e.g., the asthenosphere), but not strong enough to suppress plume formation, allows the effect of plumes to be explored.

[31] Using H = 30 (which corresponds to 50% internal heating based on bottom and surface heat flux), and an isothermal bottom boundary condition, the mantle heats up enough to form a comparable temperature and viscosity profile to internally heated cases, and form plumes. These models show plate-like behavior very similar to purely internally heated results (Figure 10b). With $Ra_D = 1.9 \times 10^6$, which corresponds to an $Ra_D^H = 7 \times 10^6$, a plate-like surface with a degree one pattern forms, with the downwelling nearly identi-

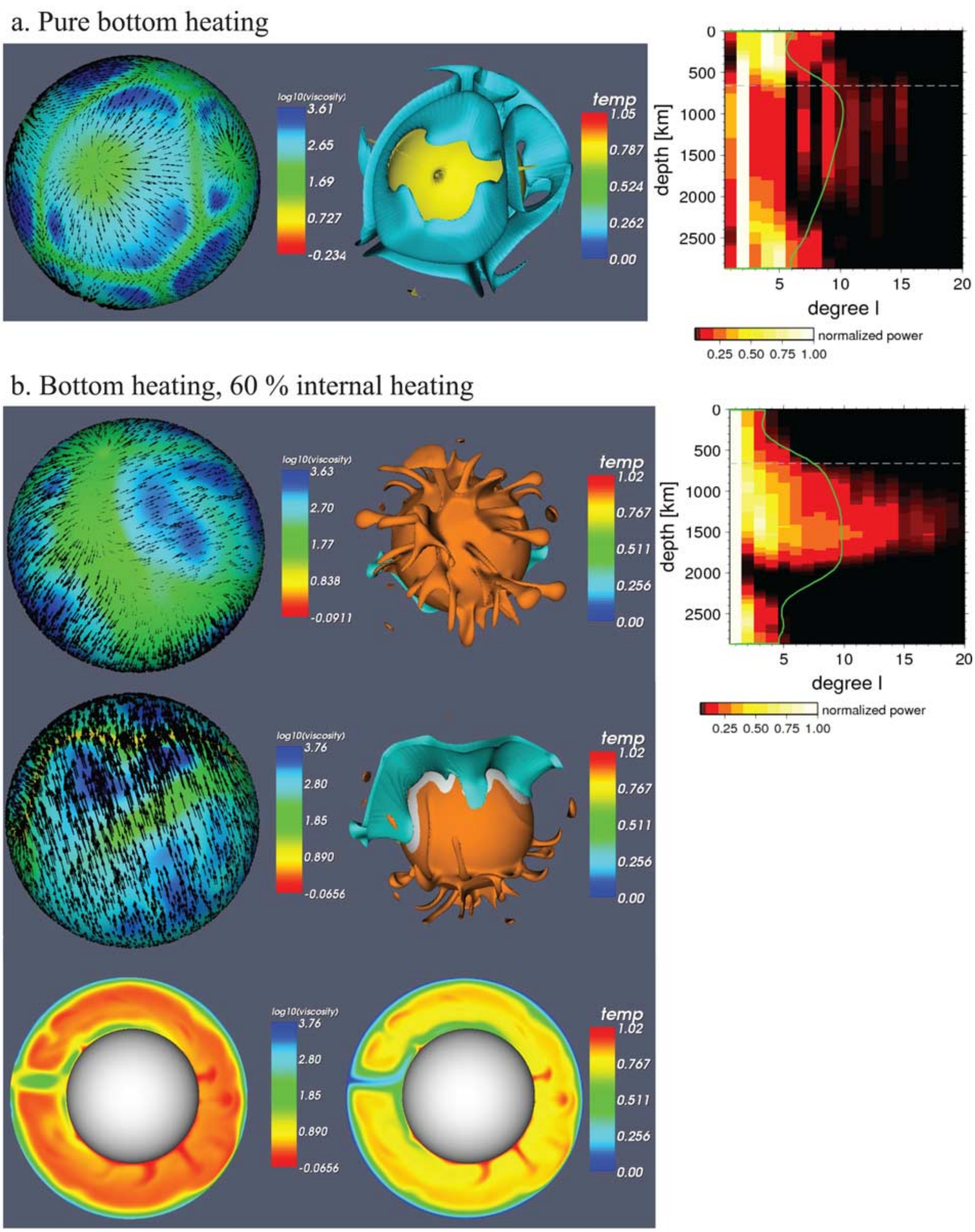

Figure 10. Convective planform images for (a) the purely bottom heated case and (b) the mixed heating (50% internally heated) case. All images in Figure 10b are from the same time step, showing the planform from different angles.

cal to the purely internally heated case. On the opposite side of the globe, numerous plumes coalesce in the upper mantle to form a large, low-viscosity layer underneath the spreading ridge. The spreading center is about three times wider than those formed by pure internal heating, and the viscosity is higher within the ridge, showing that deformation is not focusing as strongly.

3.2.4. Asthenospheric Rheology

[32] Given the importance of a low-viscosity zone underlying the top boundary layer [e.g., *Richards et al.*, 2001; *Hoeink and Lenardic*, 2008], an asthenosphere was added after *van Heck and Tackley* [2008], as a factor of 10 viscosity reduction where the temperature is near the solidus:

$$\eta(z, T) = \eta(T) \text{ if } T < T_{sol0} + 2(1 - z) \tag{12}$$

$$\eta(z, T) = 0.1\eta(T) \text{ if } T \geq T_{sol0} + 2(1 - z) \tag{13}$$

where z is the depth coordinate normalized to equal 1 at the CMB and 0 at the surface, and T_{sol0}, the surface solidus temperature was set to 0.6. Thus the viscosity reduction comes into effect mainly under spreading ridges.

[33] The addition of the "asthenosphere" significantly sharpens the zone of deformation associated with spreading ridges, making the model overall more plate-like. Other diagnostics are not strongly affected on the basis of the limited tests run with this rheology. Low *Ra* models show strong degree one patterns and moderate σ_y, high *Ra* models show more degree two patterns, as before.

4. Discussion

4.1. *Ra*-σ_y Phase Space

[34] Substantiating results by *van Heck and Tackley* [2008], larger σ_y values lead to plate-like convection as compared to Cartesian models. At a comparable Ra_D, we find a relatively similar plate-like regime, though our results show stagnant behavior for slightly lower σ_y. Furthermore, when Rayleigh number is increased, the σ_y range for plate-like behavior shifts to higher nondimensional values in a roughly linear fashion. However, when these are scaled using different reference viscosities for different Ra_D (as described in 2.1), the σ_y range for plate-like behavior is largely unaffected by Rayleigh number. The regimes described in 3.2.1 appear to be independent of *Ra*.

4.2. Wavelength

[35] In accord with *van Heck and Tackley* [2008] and *Yoshida* [2008], our results show that the wavelength of convection using a viscoplastic rheology is controlled by σ_y, though we find that *Ra* is important as well, and that shorter-wavelength structures are relatively stable through time for appropriate parameters. Models with an asthenospheric rheology showed no wavelength differences, and heating modes were not tested within as large a parameter space. Previous studies have shown that for temperature-dependent viscosity constrained by observations of Earth's viscosity structure, degree one convection dominates for all *Ra*, and that continental cover may impose a degree two pattern [*Zhong et al.*, 2007]. Furthermore, temperature-dependent viscosity convection has been shown to form shorter-wavelength structures when the extended Boussinesq approximation is used [*Yoshida*, 2008], though *Roberts and Zhong* [2006] found degree one structures for extended Boussinesq models with a wide range of radial viscosity structures.

[36] Though the majority of our models form a degree one pattern, models with high *Ra* and low σ_y show relatively stable degree two convection for constant σ_y experiments, indicating that strengthening the upper boundary layer can mask the shorter wavelengths one would expect from increasing *Ra*. For this reason these models do not produce surface motions as plate-like as models at low *Ra*, which are predominantly degree one. This is not the case with depth-dependent yield stress, where shorter-wavelength, plate-like behavior is obtained. Most models favor degree two convection, and there is significantly more power at higher degrees. This points to the surficial weakening effect of plasticity, enhanced by depth-dependent yield stress, being a key factor in allowing shorter-wavelength structures to form in strongly temperature-dependent models. Supercontinents also have a strong effect, as shown by *Zhong et al.* [2007], so combining continental dynamics with viscoplastic rheology is an important future step in understanding how Earth's wavelength patterns form.

[37] Tomographic studies show the mantle has a strong degree two convection pattern [e.g., *Becker and Boschi*, 2002]. Focusing on the midmantle, where compositional effects may be small [e.g., *Tackley*, 2002], power spectra from our degree two models correspond quite well with power spectra from tomography. In the upper 400 km, the tomographic spectrum shows more heterogeneity than our models, likely because of the differences between oceanic and continental lithosphere, which are not

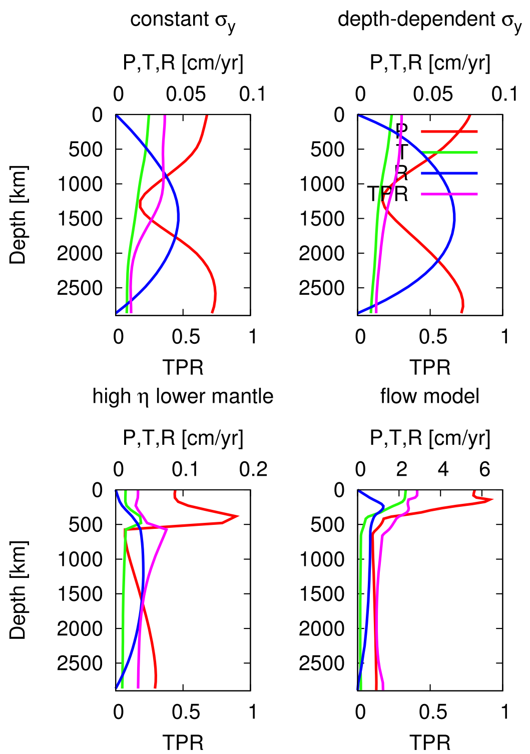

Figure 11. Poloidal, toroidal, and radial velocity (P, T, and R) and TPR with depth for models with (top left) a constant σ_y, (top right) depth-dependent σ_y, (bottom left) a two order of magnitude higher viscosity lower mantle, and (bottom right) a circulation model after *Becker* [2006].

present in our chemically homogeneous models. Through the midmantle, where both tomography and our models are dominated by slabs, there is good agreement between the models and the Earth. Near the CMB, our models show more high-degree structure than tomography does. The heterogeneity in our models is associated with downwellings piling cold material at the CMB, while on Earth it is thought to be at least partially related to chemical piles [e.g., *McNamara and Zhong*, 2005]. Adding chemical heterogeneity to convection simulations could aid in matching power spectra more closely. However, the main features can apparently be reproduced for chemically homogeneous plate-like convection simulations, and without having to invoke an increase in viscosity at 660 km depth [e.g., *Bunge et al.*, 1996], which may further increase the dominance, and perhaps stability, of degree two power.

4.3. Toroidal-Poloidal Ratios

[38] TPR trends show that spherical models have higher TPRs on average than Cartesian models, and that there is a weak *Ra* dependence over the limited range we were able to study. The increase in toroidal motion over Cartesian models is expected, as even isoviscous convection forms some toroidal motion because of spherical geometry. The *Ra* effect stems from causing more downwellings, which increases the lateral viscosity variations. When compared to the Earth, even the highest TPR models fall lower than the average TPR for the past 120 Ma [*Lithgow-Bertelloni et al.*, 1993], ∼0.55, though individual data points do reach 0.5 to 0.6. However, we cannot resolve short time scale fluctuations at the appropriate *Ra* at present. Also, TPR with these models may be increased by increasing the *Ra*, such that lateral viscosity variations are enhanced; currently unattainable within our time and computing restraints.

[39] Depth-dependent σ_y models are more plate-like than constant σ_y models, though they have lower TPRs on average, because of the reduction in lateral viscosity variations. Similar to constant σ_y models, increasing *Ra* has a weak effect on TPR, so the most plate-like model would likely have a higher viscosity contrast and higher Rayleigh number to provide the maximum lateral viscosity variation. This could also be achieved by increasing the cohesion term to make the surface stronger, but it must stay well below the ductile yield stress otherwise the whole mantle will be governed by essentially one σ_y. However, TPR seems to be increased by confining yielding to the upper mantle, because of the stabilization of the convective planform that results from this rheology.

[40] This effect indicates that near surface lateral viscosity variations are most important for exciting toroidal motion [e.g., *Tackley*, 2000b]. When TPR, as defined above on the basis of horizontal velocities, is plotted with depth, it shows a large increase to ∼1 at the midmantle. When we included the radial velocity, which is maximum at midmantle depths, TPR shows a steady decrease with depth, as do T and P velocities (Figure 11). This result is similar to *Tackley* [2000b], but somewhat different from what circulation models based on seismic tomography predict [*Becker*, 2006].

4.4. Plate-Like Quality

[41] Just how "plate-like" our models are is difficult to assess, not least because the temporal variability of plate tectonics on Earth is not well established. However, higher *Ra* models have higher TPRs and more Earth-like convective wavelength patterns, but lower plateness, though plateness is somewhat improved when adding the

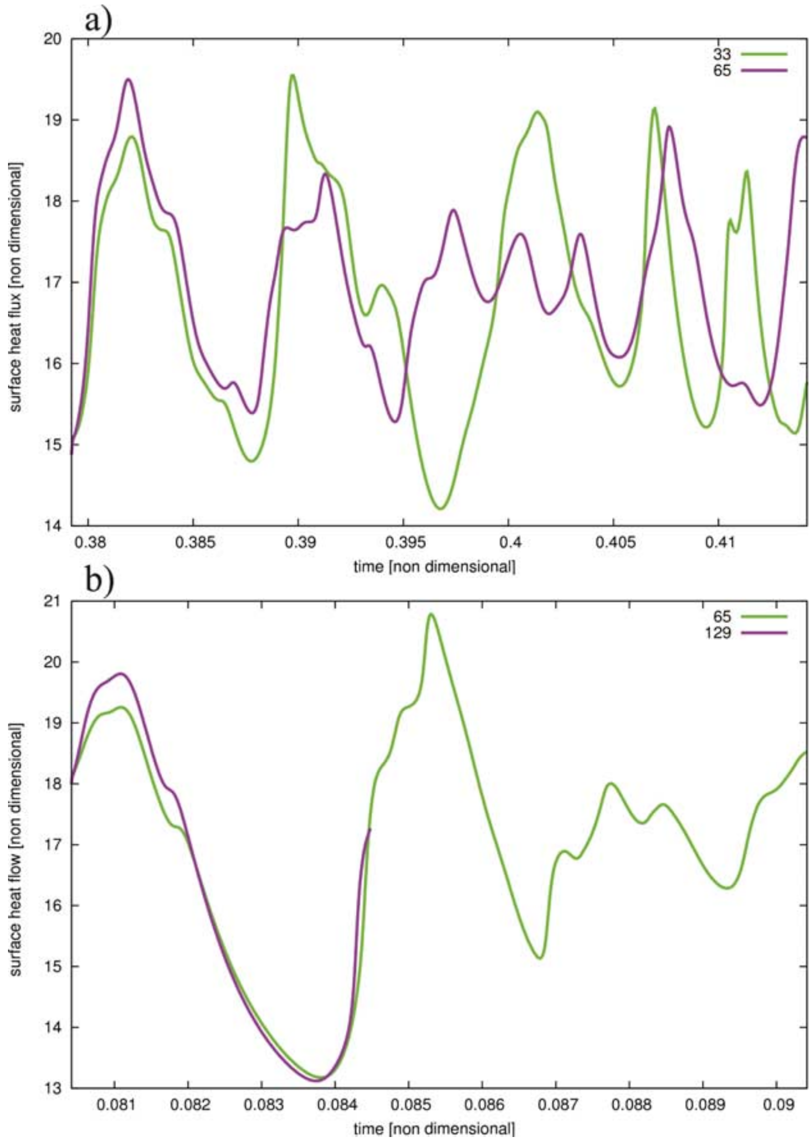

Figure A1. Surface heat flow for (a) a low Ra_D model at resolutions of 32 × 32 × 32 × 12 and 64 × 64 × 64 × 12 and (b) a high Ra_D model at resolutions of 64 × 64 × 64 × 12 and 128 × 128 × 128 × 12.

asthenosphere. Depth-dependent σ_y increases plateness and convective wavelength, but decreases TPR. Therefore the ideal model would preserve the high viscosity of the upper boundary layer, yet include a mechanism for more focused deformation. A model with some "memory" could be key for preserving plateness, yet increasing TPR and wavelength to Earth-like levels.

[42] Using bottom heating also has a significant effect as plume formation tends to "destroy" surface plates, although this effect will likely be less pronounced for compressible convection. Adding a portion of internal heating such that a low-viscosity zone forms below the top boundary layer mitigates the strong plume interaction and allows plates to form in the presence of plumes. Plates in these models form sharp downwellings, but more diffuse spreading ridges. This would likely be improved by adding the asthenospheric rheology to this case as well. These results indicate that a low-viscosity zone is crucial to plate formation, as argued by *Richards et al.* [2001], and that heating mode has a strong effect on forming such a zone. A significant portion of internal heating, ~50% for our models, is required to form a low-viscosity zone and plate-like surface when bottom heating is used.

5. Conclusions

[43] Viscoplastic, spherical convection models produce relatively plate-like surface motions for yield

stress values that are roughly constant with Rayleigh number, but fall below experimental values for rock failure. Temperature heterogeneity spectra are found to be similar to those of seismic tomography because of the organizing effect of the plates, and no radial viscosity variations or strong effect of composition appears to be required, though these effects could be important. However, there is still a significant phase space that needs to be explored to see how trends in TPR, wavelength, and plateness develop with increased *Ra*. Moreover, we need to study the effect of additional radial viscosity variations [e.g., *Bunge et al.*, 1996] and the effect of continents on viscoplastic models [*Zhong et al.*, 2007] further. Though experiments with higher Rayleigh number, viscosity contrast, and more finely tuned depth-dependent σ_y may produce plate-like results with higher TPR, our results indicate a damage or memory rheology may be needed to produce Earth-like TPR values and form true strike-slip faults.

Appendix A: Resolution Tests

[44] Resolution tests for one low Ra_D model and one high Ra_D model were performed using doubled resolution for each case, as described in section 2.1. The resolution tests show that doubling the resolution causes no significant differences in the general trends and values of key observables, such as surface heat flux (Figure A1). These models are highly time-dependent, so we do not expect results at different resolutions to agree exactly, but the general dynamics do agree, confirming our choice of resolution.

Acknowledgments

[45] We thank reviewers Shijie Zhong and Scott King; an anonymous reviewer; and the editor, Peter van Keken, for their comments, which greatly improved the manuscript. We also thank S. Zhong, E. Tan, L. Moresi, and CIG for sharing the CitcomS software.

References

Becker, T. (2006), On the effect of temperature and strain-rate dependent viscosity on global mantle flow, net rotation, and plate driving forces, *Geophys. J. Int.*, *167*, 943–957, doi:10.1111/j.1365-246X.2006.03172.x.

Becker, T., and L. Boschi (2002), A comparison of tomographic and geodynamic mantle models, *Geochem. Geophys. Geosyst.*, *3*(1), 1003, doi:10.1029/2001GC000168.

Bercovici, D. (1993), A simple model of plate generation from mantle flow, *Geophys. J. Int.*, *114*, 635–650, doi:10.1111/j.1365-246X.1993.tb06993.x.

Bercovici, D. (2003), The generation of plate tectonics from mantle convection, *Earth Planet. Sci. Lett.*, *205*, 107–121, doi:10.1016/S0012-821X(02)01009-9.

Bercovici, D., G. Schubert, and G. A. Glatzmaier (1989), Three-dimensional thermal convection in a spherical shell, *Science*, *244*, 950–955, doi:10.1126/science.244.4907.950.

Bercovici, D., Y. Ricard, and M. Richards (2000), The relation between mantle dynamics and plate tectonics: A primer, in *The History and Dynamics of Global Plate Motions*, *Geophys. Monogr. Ser.*, vol. 121, edited by M. A. Richards, R. G. Gordon, and R. D. van der Hilst, pp. 5–46, AGU, Washington, D. C.

Bunge, H. P., M. A. Richards, and J. R. Baumgardner (1996), Effect of depth-dependent viscosity on the planform of mantle convection, *Nature*, *379*, 436–438, doi:10.1038/379436a0.

Busse, F. H., M. A. Richards, and A. Lenardic (2006), A simple model of high Prandtl and high Rayleigh number convection bounded by thin low viscosity layers, *Geophys. J. Int.*, *164*, 160–167, doi:10.1111/j.1365-246X.2005.02836.x.

Chen, J., and S. King (1998), The influence of temperature and depth dependent viscosity on geoid and topography profiles from models of mantle convection, *Phys. Earth Planet. Inter.*, *106*, 75–92, doi:10.1016/S0031-9201(97)00110-6.

Christensen, U. (1984), Convection with pressure-dependent and temperature-dependent non-Newtonian rheology, *Geophys. J. R. Astron. Soc.*, *77*, 343–384.

Davies, G. E. (1999), *Dynamic Earth: Plates, Plumes and Mantle Convection*, Cambridge Univ. Press, Cambridge, U. K.

Han, L., and M. Gurnis (1999), How valid are dynamics models of subduction and convection when plate motions are prescribed?, *Phys. Earth Planet. Inter.*, *110*, 235–246, doi:10.1016/S0031-9201(98)00156-3.

Hoeink, T., and A. Lenardic (2008), Three-dimensional mantle convection simulations with a low-viscosity asthenosphere and the relationship between heat flow and the horizontal length scale of convection, *Geophys. Res. Lett.*, *35*, L10304, doi:10.1029/2008GL033854.

King, S. D., and B. H. Hager (1990), The relationship between plate velocity and trench viscosity in Newtonian and power-law subduction calculations, *Geophys. Res. Lett.*, *17*, 2409–2412, doi:10.1029/GL017i013p02409.

Kohlstedt, D. L., B. Evans, and S. J. Maxwell (1995), Strength of the lithosphere-constraints imposed by laboratory experiments, *J. Geophys. Res.*, *100*, 17,587–17,602, doi:10.1029/95JB01460.

Lay, T., J. Hernlund, and B. Buffett (2008), Core-mantle boundary heat flow, *Nat. Geosci.*, *1*, 25–32, doi:10.1038/ngeo.2007.44.

Lithgow-Bertelloni, C., M. A. Richards, Y. Ricard, R. O'Connell, and D. Engebretson (1993), Toroidal-poloidal partitioning of plate motions since 120 Ma, *Geophys. Res. Lett.*, *18*, 1751–1754.

Masters, G., T. H. Jordan, P. G. Silver, and F. Gilbert (1982), Aspherical Earth structure from fundamental spheroidal mode data, *Nature*, *298*, 609–613, doi:10.1038/298609a0.

McKenzie, D. P., and W. J. Morgan (1969), Evolution of triple junctions, *Nature*, *224*, 125–133, doi:10.1038/224125a0.

McNamara, A. K., and S. Zhong (2005), Thermochemical structures beneath Africa and the Pacific Ocean, *Nature*, *437*, 1136–1139, doi:10.1038/nature04066.

Megnin, C., H.-P. Bunge, B. Romanowicz, and M. A. Richards (1997), Imaging 3-D spherical convection models: What can seismic tomography tell us about mantle dynamics?, *Geophys. Res. Lett.*, *24*, 1299–1302, doi:10.1029/97GL01256.

Moresi, L., and V. Solomatov (1995), Numerical investigation of 2D convection with extremely large viscosity variations, *Phys. Fluids*, *7*, 2154–2161, doi:10.1063/1.868465.

Moresi, L., and V. Solomatov (1998), Mantle convection with a brittle lithosphere-thoughts on the global tectonic styles of the Earth and Venus, *Geophys. J. Int.*, *133*, 669–682, doi:10.1046/j.1365-246X.1998.00521.x.

Ogawa, M., G. Schubert, and A. Zebib (1991), Numerical simulations of 3-dimensional thermal convection in a fluid with strongly temperature dependent viscosity, *J. Fluid Mech.*, *233*, 299–328, doi:10.1017/S0022112091000496.

Ricard, Y., M. A. Richards, C. Lithgow-Bertelloni, and Y. LeStunff (1993), A geodynamical model of mantle density heterogeneity, *J. Geophys. Res.*, *98*, 21,895–21,909, doi:10.1029/93JB02216.

Richards, M. A., W.-S. Yang, J. Baumgardner, and H.-P. Bunge (2001), Role of a low-viscosity zone in stabilizing plate tectonics: Implications for comparative terrestrial planetology, *Geochem. Geophys. Geosyst.*, *2*(8), 1026, doi:10.1029/2000GC000115.

Ritsema, J., H. J. van Heijst, and J. H. Woodhouse (2004), Global transition zone tomography, *J. Geophys. Res.*, *109*, B02302, doi:10.1029/2003JB002610.

Ritsema, J., A. K. McNamara, and A. L. Bull (2007), Tomographic filtering of geodynamical models: Implications for model interpretation and large scale mantle structure, *J. Geophys. Res.*, *112*, B01303, doi:10.1029/2006JB004566.

Roberts, J. H., and S. Zhong (2006), Degree-1 convection in the Martian mantle and the origin of the hemispheric dichotomy, *J. Geophys. Res.*, *111*, E06013, doi:10.1029/2005JE002668.

Schott, B., and H. Schmelling (1998), Delamination and detachment of a lithospheric root, *Tectonophysics*, *296*, 225–247, doi:10.1016/S0040-1951(98)00154-1.

Solomatov, V. (1995), Scaling of temperature-dependent and stress-dependent viscosity convection, *Phys. Fluids*, *7*, 266–274, doi:10.1063/1.868624.

Stein, C., J. Schmalzl, and U. Hansen (2004), The effect of rheological parameters on plate behaviour in a self-consistent model of mantle convection, *Phys. Earth Planet. Inter.*, *142*, 225–255, doi:10.1016/j.pepi.2004.01.006.

Su, W.-J., and A. M. Dziewonski (1991), Predominance of long-wavelength heterogeneity in the mantle, *Nature*, *352*, 121–126, doi:10.1038/352121a0.

Tackley, P. (1996), On the ability of phase transitions and viscosity layering to induce long-wavelength heterogeneity in the mantle, *Geophys. Res. Lett.*, *23*, 1985–1988, doi:10.1029/96GL01980.

Tackley, P. (2000a), Self-consistent generation of tectonics plates in time-dependent, three-dimensional mantle convection simulations: 1. Pseudoplastic yielding, *Geochem. Geophys. Geosyst.*, *1*(8), 1021, doi:10.1029/2000GC000036.

Tackley, P. (2000b), Self-consistent generation of tectonic plates in time-dependent, three-dimensional mantle convection simulations: 2. Strain weakening and asthenosphere, *Geochem. Geophys. Geosyst.*, *1*(8), 1026, doi:10.1029/2000GC000043.

Tackley, P. (2000c), The quest for self-consistent generation of plate tectonics in mantle convection models, in *The History and Dynamics of Global Plate Motions*, *Geophys. Monogr. Ser.*, vol. 121, edited by M. Richards, R. Gordon, and R. D. Van der Hilst, pp. 47–72, AGU, Washington, D. C.

Tackley, P. (2002), Strong heterogeneity caused by deep mantle layering, *Geochem. Geophys. Geosyst.*, *3*(4), 1024, doi:10.1029/2001GC000167.

Tan, E., E. Choi, P. Thoutireddy, M. Gurnis, and M. Aivazis (2006), GeoFramework: Coupling multiple models of mantle convection within a computational framework, *Geochem. Geophys. Geosyst.*, *7*, Q06001, doi:10.1029/2005GC001155.

Trompert, R., and U. Hansen (1998), Mantle convection simulations with rheologies that generate plate-like behavior, *Nature*, *395*, 686–689, doi:10.1038/27185.

van Heck, H. J., and P. Tackley (2008), Planforms of self-consistently generated plates in 3D spherical geometry, *Geophys. Res. Lett.*, *35*, L19312, doi:10.1029/2008GL035190.

Walzer, U., and R. Hendel (2008), Mantle convection and evolution with growing continents, *J. Geophys. Res.*, *113*, B09405, doi:10.1029/2007JB005459.

Weinstein, S. A., and P. L. Olson (1992), Thermal convection with non-Newtonian plates, *Geophys. J. Int.*, *111*, 515–530, doi:10.1111/j.1365-246X.1992.tb02109.x.

Yoshida, M. (2008), Mantle convection with longest-wavelength thermal heterogeneity in a 3-D spherical model: Degree one or two?, *Geophys. Res. Lett.*, *35*, L23302, doi:10.1029/2008GL036059.

Zhong, S. (2001), Role of ocean-continent contrast and continental keels on plate motion, net rotation of the lithosphere, and the geoid, *J. Geophys. Res.*, *106*, 703–712, doi:10.1029/2000JB900364.

Zhong, S., M. Gurnis, and L. Moresi (1998), Role of faults, non-linear rheology, and viscosity structure in generating plates from instantaneous mantle flow models, *J. Geophys. Res.*, *103*, 15,255–15,268, doi:10.1029/98JB00605.

Zhong, S., M. Zuber, L. Moresi, and M. Gurnis (2000), The role of temperature-dependent viscosity and surface plates in spherical shell models of mantle convection, *J. Geophys. Res.*, *105*, 11,063–11,082, doi:10.1029/2000JB900003.

Zhong, S., N. Zhang, L. Zheng-Xiang, and J. Roberts (2007), Supercontinent cycles, true polar wander, and very long-wavelength mantle convection, *Earth Planet. Sci. Lett.*, *261*, 551–564, doi:10.1016/j.epsl.2007.07.049.